Contact Resistance Properties between Nanotubes and Various Metals from Quantum Mechanics

Yuki Matsuda, Wei-Qiao Deng,† and William A. Goddard, III*

Materials and Process Simulation Center, Division of Chemistry and Chemical Engineering, Beckman Institute 139-74, and Department of Materials Science, Division of Engineering and Applied Science, California Institute of Technology, Pasadena, California 91125

Received: April 10, 2007; In Final Form: May 18, 2007

We report on the interfacial structure, the current−voltage ($I-V$) characteristics, and contact resistance of metal electrode−carbon nanotube contacts for five metals, Ti, Pd, Pt, Cu, and Au, based on first-principles quantum mechanical density functional and matrix Green's function methods. We find that Ti leads to the lowest contact resistance followed by Pd, Pt, Cu, and Au. The sequence, Ti ≫ Pd > Pt > Cu > Au, correlates well with the predicted cohesive strength of the electrode−carbon interface. In addition Ti leads to linear $I-V$ characteristics up to ∼1 V, suggesting an Ohmic contact for both metallic and semiconductor nanotubes. However, the high reactivity of the Ti electrode at the contact to the nanotube distorts the nanotube structure.

Carbon nanotubes are promising candidates for nanoelectronic devices due to their unique structural and electrical properties. Indeed, much experimental progress toward electronic devices based on carbon nanotubes has been reported.[1−12] In particular, near ballistic transport properties have been reported for both single-walled carbon nanotubes (SWNTs)[1,2] and multiwalled carbon nanotubes (MWNTs).[10] A potential problem with these devices is the high contact resistance, which significantly influences the conductance although it is hard to extract experimentally due to the variation in device geometries.

Several metals have been studied experimentally as candidates for ideal Ohmic contacts to carbon nanotubes,[1−12] but the experiments have given statistically inconsistent results due to difficulties in the fabrication of a large number of statistically representative carbon nanotube/metal contacts. Recent experimental results suggested that Pd and Ti contacts are superior to Au and Pt contacts,[1−9] but the results for Ti are erratic possibly due to the high chemical reactivity of Ti compared to other metals.[9,12] For example, annealing the Ti−carbon nanotube interface at temperatures above 973 K led to formation of titanium carbide at the interface.[12] Theoretical studies have been reported for the geometric structures of carbon nanotubes with "side-contacted" and "end-contacted" metal electrodes.[13−18] However, none of these studies reported the $I-V$ relationships (resistance) of metal−nanotube contacts although the Schottky barrier height between a metal surface (Pd, Pt, or Au) and a nanotube was reported.[14] We chose to simulate side-contacted nanotube models because current fabrication technology does not allow for the construction of end-contacted devices. We first considered the local structure, $I-V$ characteristics, and contact resistance from first-principles calculations on five metals (Ti, Pd, Pt, Cu, and Au) by depositing them on simple graphene surfaces to choose the best contact metals for nanotubes. We then used the best two candidate metals for investigating more realistic metal−nanotube models.

Our procedure was to start with a 2 × 2 unit cell (8 carbons per layer) of the graphite surface (fixed at 4.89 × 4.89 Å^2) and used quantum mechanics to optimize the periodic metal layers. We placed the atoms one by one, followed by relaxing the geometry each time to represent the deposited metal on the graphite surface. We used SEQQUEST,[19] a fully self-consistent Gaussian-based linear combination of atomic orbitals (LCAO) density functional theory (DFT) method with double-ζ plus polarization (DZP) basis sets.[20] All calculations were based on the Perdew−Burke−Ernzerhof generalized gradient approximation (GGA) with Perden−Burke−Emzarhof (PBE) pseudoatomic potentials and spin polarization within two-dimensional periodic boundary conditions.[21] The k-point sampling of 4 × 4 in the Brillouin Zone and the real space grid interval of 32 × 32 in the $x-y$ plane, for a grid spacing of 0.25/point, were carefully determined by energetic convergence.

In each case, we found approximately close-packed layers of metal (three atoms per layer per cell) with ABC stacking (face-centered cubic (fcc)) for Pd, Pt, Cu, and Au and ABAB stacking (hexagonal close-packed (hcp)) for Ti, just as expected for the bulk structures. For Ti fcc packing was found to be less stable than hcp structure by 1.2 kcal/mol per unit cell. Figures 1a and 1b show the top views and side views of the models of Ti and Pd deposited on a 4 × 4 graphene sheet. For each system the metal−metal distances within each layer are within 10% of the nearest neighbor distances of the bulk crystal structure. Importantly, the distance between graphene and the first deposited metal layer is quite small for Ti (strong bonding) and increases as Pd < Pt < Cu < Au (Table 1). The interaction energy of each metal−graphene model was calculated by changing the distance at the interface using the single-point energy calculation (Figure 1c). Figure 1c showed that the Ti layers bind strongly with graphene (48.3 kcal/mol per unit cell), while the cohesion for the other metals is much weaker, decreasing as Pd > Pt > Cu > Au, inversely correlated with the metal−graphene layer distance.

To compare directly the contact resistance at the interface between each metal and graphene sheet, $I-V$ models were constructed from the optimized geometries (Figures 1a and 1b) by reversing one of the models and placing it at the AB stacking

* Author to whom correspondence should be addressed. Phone: (626) 395-2731; (626) 395-2730 (Secretary). Fax: (626) 585-0918. E-mail: wag@wag.caltech.edu.

† Current address: Division of Chemistry and Biological Chemistry, School of Physical and Mathematical Sciences, Nanyang Technological University, Singapore 639798, Singapore.

10.1021/jp072794a CCC: $37.00
Published on Web 07/03/2007

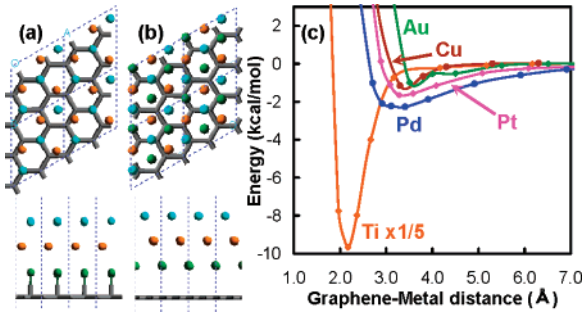

Figure 1. Optimized geometries of the top (top) and side (bottom) views of (a) Ti and (b) Pd deposited on a graphene 4 × 4 sheet. (Unit cell for optimization is a graphene 2 × 2 sheet) (gray, graphite; green, metal first layer; orange, metal second layer; light blue, metal third layer). (c) Interaction energy of the metal−graphene model. Ti was scaled by 1:5 (orange, Ti; blue, Pd; pink, Pt; brown, Cu; green, Au).

positions of the original graphene sheet (Figures 2a and 2b). These models represent the two contacts (source and drain) of a nanotube. The distance between the two graphene sheets was fixed at 3.4 Å, which is specified by the experimental data.[20] Using these metal−graphene−metal configurations, we calculated the current as a function of voltage to compare the contact resistance of the five deposited metals. First we calculated the projected density of state (PDOS) from DFT quantum mechanics, and then we calculated the transmission coefficient using nonequilibrium Green's function theory with DFT (which we have used successfully to compute transport properties of molecular electronic devices).[23,24] The transmission function was then used in the Landauer−Buttiker formula to calculate the $I-V$ characteristics. The total resistance of these systems was then obtained from the zero-bias transmission.

The PDOS of the pπ orbitals of the graphene carbon atoms is shown in Figure 2c while the PDOS for the d-orbitals of the first-layer metal atoms (the layer closest to the graphene) is shown in Figure 2d. (The PDOS of other orbitals of carbon and the metals are not shown since their values did not contribute significantly.) For the Ti model, the d PDOS of Ti and the pπ PDOS of carbon are large and uniform, indicating a good conduction channel. The Pd and Pt models showed the second and third highest combinations of metal d PDOS and graphene pπ PDOS. For the Cu and Au models the pπ PDOS shows many peaks or resonances, indicating electronic weak coupling of the metal with graphene. This behavior in the PDOS correlates directly with the metal carbon bond strength (Table 1): Ti ≫ Pd > Pt > Cu > Au. The transmission function (Figure 2e) near the Fermi energy is mirroring the PDOS behaviors. In turn, the $I-V$ characteristics (Figure 2f) and total resistance per square nanometer (Figure 2g) correlate directly with the transmission coefficient and hence correlate with the cohesive coupling between metal d-orbitals and the graphite pπ orbitals as discussed above. The bias voltage is defined as the difference between the source and the drain voltage.

We find that Ti has a linear $I-V$ curve indicating an Ohmic contact. We calculate contact resistances of 24.2 kΩ/nm^2 for Ti, 221 kΩ/nm^2 for Pd, 881 kΩ/nm^2 for Pt, 16.3 MΩ/nm^2 for Cu, and 32.6 MΩ/nm^2 for Au after averaging the bias voltage from −0.1 to +0.1 V. These values should be interpreted as a relative evaluation of these metals. Thus, on the basis of the graphene−metal model studies, we conclude that for metals deposited on carbon nanotubes the contact resistance is the lowest for Ti, followed by Pd, Pt, Cu, and Au.

Next, we selected Ti and Pd, the best two candidates as contact materials, for calculations using more realistic metal−nanotube−metal assemblies. We placed the metallic SWNT (7,7), with diameter of 9.6 Å, between a pair of metal triple layers (Ti or Pd), keeping the periodic configurations of metal atoms on the graphene sheet and minimum distances at the electrode−nanotube interface obtained from the metal−graphene calculations. The geometries were minimized just as for the metal−graphite system using one-dimensional periodic boundary conditions (Figures 3a and 3b, where the top two layers were kept fixed). After optimization, we calculated the metal electrode−nanotube distance, cohesive energy, and strain energy in the SWNTs (compared to its original SWNT structure) (Table 2). For both systems, the distance between the nanotube and electrodes became 0.04−0.08 Å (1.9−2.8%) smaller than that in the graphene case, indicating the larger attractive interaction due to the incursion of s hybrid character in the pπ orbital caused by the curvature of the nanotube. We find a similar ratio of the distance at the metal−nanotube interface as for metal−graphene (Ti/Pd = 0.75 in the graphene case and 0.75 for SWNT (7,7)), indicating that the graphite model represents the nanotube for geometric considerations.

The PDOS and the transmission functions of the Ti− or Pd−SWNT (7,7) are shown in Figures 3e and 3f, respectively. As expected from the metal−graphene studies, for Ti−SWNT (7,7), we find a strong coupling to the carbon pπ orbitals but much weaker for Pd−SWNT (7,7). The $I-V$ characteristics and contact resistance are shown in Figures 3g and 3h, respectively. The $I-V$ characteristics of Ti−SWNT (7,7) show linearity

TABLE 1: Layer−Layer distance of the Metal−Graphene Models after Optimization (Å) and Cohesive energy (kcal/mol) of the Interface between Metal and Graphene[a]

	Ti	Pd	Pt	Cu	Au
graphene−first metal layer distance (Å)	2.17	2.91	3.38	3.30	3.50
first metal layer−second metal layer distance (Å)	2.44	2.22	2.30	2.02	2.54
second metal layer−third metal layer distance (Å)	2.27	2.22	2.29	2.02	2.52
bulk value (calculated) (Å)	2.33	2.27	2.29	2.14	2.40
bulk value (experimental) 300 K[b] (Å)	2.34	2.25	2.26	2.08	2.36
calculated metal−graphene cohesive energy (kcal/mol)	48.3	2.1	1.7	1.2	1.0

[a] All calculated distances are averaged values. [b] Reference 22.

TABLE 2: Distance (Å) and Cohesive Energy (kcal/mol) between metal and SWNT Models and Strain Energy of SWNT after Optimization

	Ti−SWNT (7,7)	Pd−SWNT (7,7)	Ti−SWNT (13,0)	Pd−SWNT (13,0)
SWNT−first metal layer distance (Å)	2.13	2.83	2.11	2.74
metal−SWNT cohesive energy (kcal/mol nm)	423.5	33.5	441.9	40.6
strain energy[a] of SWNT (kcal/mol nm)	72.8	1.8	96.5	0.9

[a] Obtained by comparing it to the initial structure.

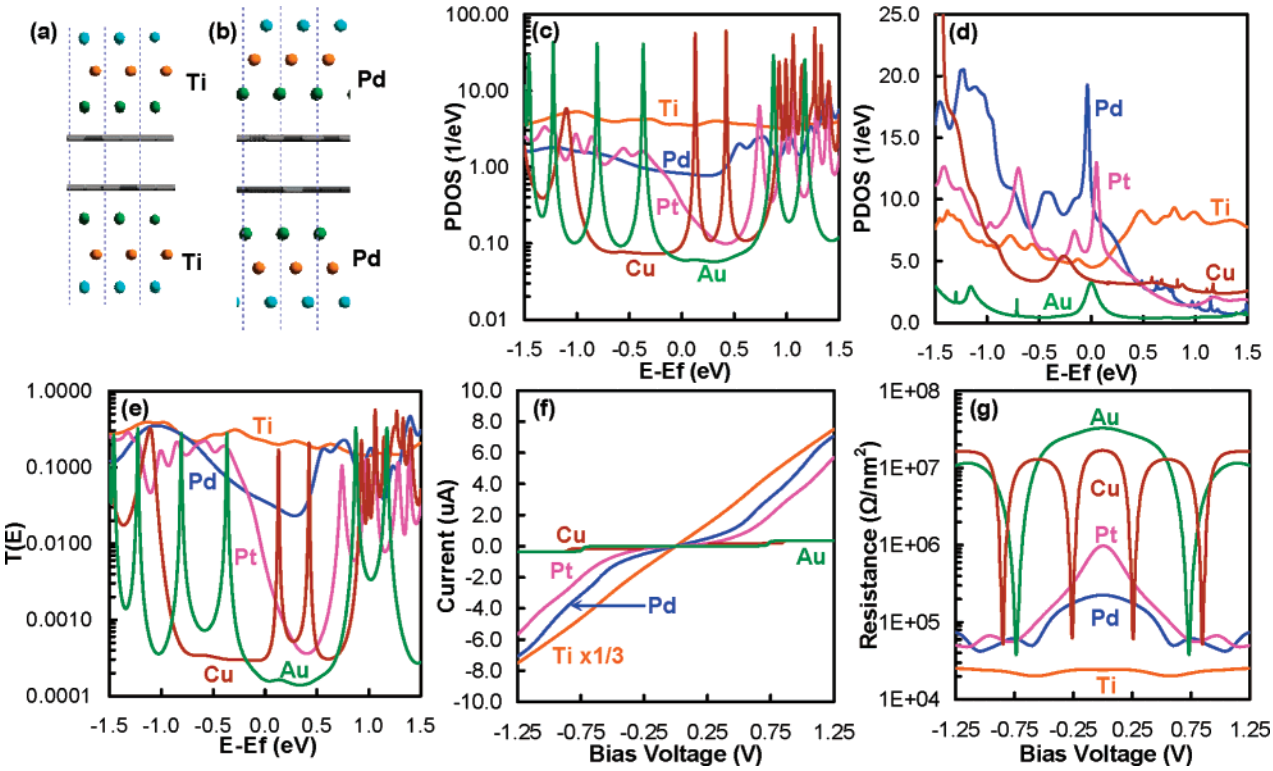

Figure 2. *I*−*V* characteristics of the metal−graphene (two sheets of AB stacking) models. Side views of *I*−*V* calculation model of (a) Ti−graphene−Ti and (b) Pd−graphene−Pd. The *I*−*V* models were constructed from the optimized models of metal−graphene (Figures 1a and 1b). (c) Projected density of states (PDOS) near the Fermi energy (E_f) of the pπ orbital of carbon in graphite (orange, Ti; blue, Pd; pink, Pt; brown, Cu; green, Au). (d) PDOS of d-orbital of metal electrodes. (e) Transmission coefficient ($T(E)$). (f) *I*−*V* curve. Ti−graphite model was scaled by 1:3. (g) Contact resistance per square nanometer at metal−graphite interface.

indicating Ohmic contact. These calculations lead to contact resistances of 6.9 kΩ/nm for Ti−SWNT (7,7) and 63.7 kΩ/nm for Pd−SWNT (7,7) after averaging bias voltages from −0.1 to 0.1 V. The contact resistance of Ti/Pd is 0.11 for graphene and 0.11 for metal nanotube.

Although the main point of this research was to determine the best metals for contacts to metallic nanotubes, we additionally considered the interface of the metal−semiconductor SWNT (13,0) with a diameter of 10.0 Å (Figures 3c and 3d). This led to similar geometries as for metallic nanotubes (the ratio of the distance at the interface is Ti/Pd = 0.77); however the Ti contacts significantly broaden the semiconductor nanotube states near the Fermi Energy, leading to a nearly metallic system as shown in Figure 3e. We expect that this would make Ti a poor candidate for the gate electrodes of carbon nanotube field-effect transistors. These calculations lead to contact resistances of 30.7 kΩ/nm for Ti−SWNT (13,0) and 1620 kΩ/nm for Pd−SWNT (13,0) after averaging bias voltages from −0.1 to 0.1 V. The contact resistance of Ti/Pd is 0.02 for semiconductor nanotubes.

In conclusion, our calculations suggest that the coupling of the metal d-orbitals of the electrode and the pπ orbitals of the carbon atoms play a critical role in determining both the cohesive and the electronic interactions at the contacts. Considering only contact resistance, the suitability of metals as electrodes for metallic carbon nanotubes descends as Ti ≫ Pd > Pt > Cu > Au. Ti forms an Ohmic contact through its strong chemical bond to carbon atoms on both metallic and semiconductor nanotubes. However, the high reactivity of Ti might also lead to oxidation of the Ti[11] or else reaction with the nanotube to form Titanium carbide (TiC).[8] We expect that our calculations provide a lower bound for contact resistances since we have assumed perfect contact geometries and no defects and have used DFT calculations with a PBE functional that underestimate

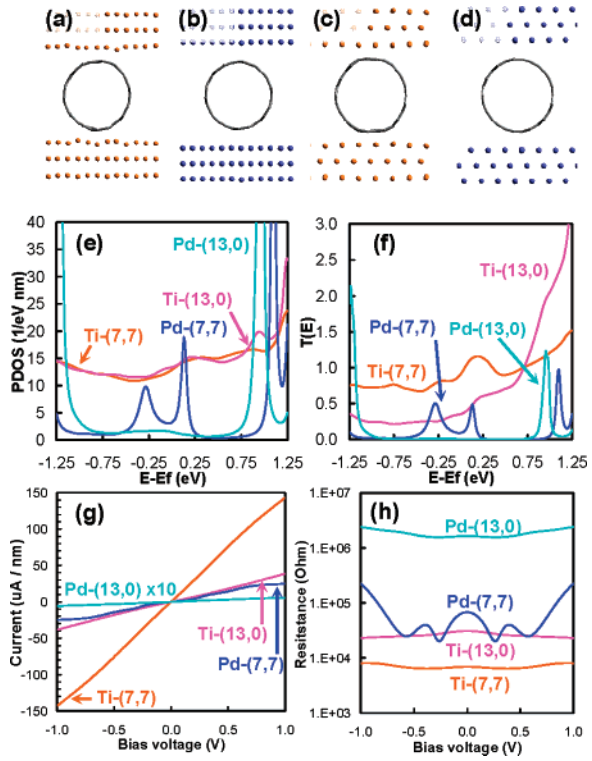

Figure 3. *I*−*V* characteristics of Ti−SWNT (7,7), Pd−SWNT (7,7), Ti−SWNT (13,0), and Pd−SWNT (13,0). Cross-sections of the *I*−*V* optimized models of (a) Ti−SWNT (7,7)−Ti, (b) Pd−SWNT (7,7)−Pd, (c) Ti−SWNT (13,0) and (d) Pd−SWNT (13,0). (e) PDOS (1/eV nm) near the Fermi energy. (f) Transmission coefficient ($T(E)$). (g) *I*−*V* curve. Pd−SWNT (13,0) was magnified by 10. (h) Contact resistance per nanometer (orange, Ti−SWNT (7,7); blue, Pd−SWNT (7,7); pink, Ti−SWNT (13,0); light blue, Pd−SWNT (13,0)).

the level of the conduction band.[25] The experimental trend that Ti and Pd are better than Pt and Au contacts[1−9] is in agreement with our calculations.

Contact metals have not been evaluated experimentally because it has been difficult to extract the contact resistance due to the variations in device geometries. Therefore, these results may provide useful guide lines for experimentalists to select the best contact materials for carbon nanotube device architectures. These studies show how first-principle predictions of complex phenomena such as contact resistance in metal−nanotube assemblies can now be effectively investigated computationally. Given the difficulty, expense, and time required for the experiments, theory may now be useful for high throughout screening to identify the best conditions and materials before performing experiments.

Acknowledgment. This work was supported by Intel Components Research (Kevin O'Brien, James M. Blackwell, and Florian Gstrein) and by the National Science Foundation (Grant Nos. CCF-0524490 and CTS-0608889). The computer systems used in the research were provided by ARO-DURIP and ONR-DURIP. Additional support for this research was provided by ONR, ARO, DOE, NIH, Chevron, Boehringer-Ingelheim, Pfizer, Allozyme, Nissan, Dow-Corning, DuPont, and MARCO-FENA.

Supporting Information Available: Optimized geometries of the top views and side views of (a) Ti, (b) Pd, (c) Pt, (d) Cu, and (e) Au deposited on a graphene 4×4 sheet. This material is available free of charge via the Internet at http://pubs.acs.org.

References and Notes

(1) Javey, A.; Guo, J.; Wang, Q.; Lundstrom, M.; Dai, H. *Nature* **2003**, *424*, 654.

(2) Mann, D.; Javey, A.; Kong, J.; Wang, Q.; Dai, H. *Nano. Lett.* **2003**, *3*, 1541.

(3) Tans, S. J.; Verschueren, A. R. M.; Dekker, C. *Nature* **1998**, *393*, 49.

(4) Rosenblatt, S.; Yaish, Y.; Park, J.; Gore, J.; Sazonova, V.; McEuen, P. L. *Nano Lett.* **2002**, *2*, 869.

(5) Seidel, R. V.; Graham, A. P.; Kretz, J.; Rajasekharan, B.; Duesberg, G. S.; Liebau, M.; Unger, E.; Kreupl, F.; Hoenlein, W. *Nano Lett.* **2005**, *5*, 147.

(6) Cui, X.; Freitag, M.; Martel, R.; Brus, L.; Avouris, P. *Nano Lett.* **2003**, *3*, 783.

(7) Austin, D. W.; Puretzky, A. A.; Geohegan, D. B.; Britt, P. F.; Guillorn, M. A.; Simpson, M. L. *Chem. Phys. Lett.* **2002**, *361*, 525.

(8) Martel, R.; Derycke, V.; Lavoie, C.; Appenzeller, J.; Chan, K. K.; Tersoff, J.; Avouris, P. *Phys. Rev. Lett.* **2001**, *87*, 256805.

(9) Marty, L.; Bouchiat, V.; Naud, C.; Chaumont, M.; Fournier, T.; Bonnot, A. M. *Nano Lett.* **2003**, *3*, 1115.

(10) Frank, S.; Poncharal, P.; Wang, Z. L.; de Heer, W. A. *Science* **1998**, *280*, 1744.

(11) Kanda, A.; Ootuka, Y.; Tsukagoshi, K.; Aoyagi, Y. *Appl. Phys. Lett.* **2001**, *79*, 1354.

(12) Martel, R.; Schmidt, T.; Shea, H. R.; Hertel, T.; Avouris, P. *Appl. Phys. Lett.* **1998**, *73*, 2447.

(13) Dag, S.; Gulseren, O.; Yildrim, T.; Ciraci, S. *Appl. Phys. Lett.* **2003**, *83*, 3180.

(14) Shan, B.; Kyeongjae, C. *Phys. Rev. B* **2004**, *70*, 233405.

(15) Tarakeshwar, P.; Kim, M. *J. Phys. Chem. B* **2005**, *109*, 7601.

(16) Pomorski, P.; Roland, C.; Guo, H. *Phys. Rev. B* **2004**, *70*, 115408.

(17) Durgun, E.; Dag, S.; Ciraci, S.; Gulseren, O. *J. Phys. Chem. B.* **2004**, *108*, 575.

(18) Anantram, M. P.; Datta, S.; Xue, Y. *Phys. Rev. B* **2000**, *61*, 14219.

(19) Schultz, P. A. *SEQQUEST Code*; Sandia National Labs: Albuquerque, NM, 2005. http://dft.sandia.gov/Quest/.

(20) Mattsson, A. E.; Schultz, P. A.; Desjarlais, M. P.; Mattsson, T. R.; Leung, K. *Modell. Simul. Mater. Sci. Eng.* **2005**, *13*, R1−R31.

(21) Perdew, J. P.; Burke, K.; Ernzerhof, M. *Phys. Rev. Lett.* **1996**, *77*, 3865.

(22) *CRC Handbook of Chemistry and Physics*, 87th ed.; Lide, D. R., Ed.; CRC Press: Boca Raton, FL, 2006.

(23) Kim, Y.-H.; Jang, S. S.; Jang, Y. H.; Goddard, W. A., III. *Phys. Rev. Lett.* **2005**, *94*, 156801.

(24) Kim, Y.-H.; Tahir-Kheli, J.; Schultz, P. A.; Goddard, W. A., III. *Phys. Rev. B* **2006**, *73*, 235419.

(25) Muscat, J.; Wander, A.; Harrison, N. M. *Chem. Phys. Lett.* **2001**, *342*, 397.